Eur Biophys J (2008) 37:759–771
DOI 10.1007/s00249-008-0258-3

ORIGINAL PAPER

Fatty acid interdigitation in stratum corneum model membranes: a neutron diffraction study

A. Ruettinger · M. A. Kiselev · Th. Hauss · S. Dante · A. M. Balagurov · R. H. H. Neubert

Received: 21 June 2007 / Revised: 4 December 2007 / Accepted: 21 December 2007 / Published online: 22 January 2008

Abstract The influence of the chain length of the free fatty acid (FFA) in a stratum corneum (SC) lipid model membrane composed of *N*-(α-hydroxyoctadecanoyl)-phytosphingosine (CER [AP]), cholesterol (Ch), FFA and cholesterol sulphate (ChS) was investigated by neutron diffraction. The internal nanostructure of the SC lipid membrane in addition to the water distribution function was determined via calculation of the neutron scattering length density profile (Fourier profile). The Fourier profiles of the studied SC model membranes revealed that such membranes have a repeat distance approximately equal to the membrane thickness. Increasing the chain length of the FFA in the CER[AP] based model membrane did not cause an alteration of the internal nanostructure but led to a decrease in the membrane repeat distance from 45.6 Å (palmitic acid, C16:0) to 43.7 Å (cerotic acid, C26:0) due to a partial interdigitation of the FFA chains. Ceramide [AP] forces the long chain fatty acids to incorporate into the unchanged spacing of the bilayer, thereby obligating the FFA protrude partly through opposing leaflet. Furthermore, the longer chained free fatty acids tend to form a new separate so-called "fatty acid rich phase". Therefore, the elongation of the chain length of the FFA decreases the solubility of the FFA in the SC model membrane based on CER[AP].

Keywords Ceramide · Stratum corneum · Lipid membrane · Fatty acids · Neutron diffraction

Abbreviations

CER [AP]	*N*-(α-gydroxyoctadecanoyl)-phytosphingosine
Ch	Cholesterol
ChS	Cholesterol sulphate
FFA	Free fatty acid
FWHH	Full width at half height
HH	Hydrophilic–hydrophobic
SA	Stearic acid
BA	Behenic acid
TA	Tetracosanoic acid
CA	Cerotic acid
RH	Relative humidity
SC	Stratum corneum
TEWL	Transepidermal water loss

Introduction

The stratum corneum (SC), which is the outermost layer of the mammalian skin, has been the in the focus of research for more than 30 years. The composition of the SC lipid matrix is completely different in comparison to cell membranes. The major lipids found in the SC are ceramides, cholesterol and its derivatives as well as free fatty acids (FFA) (Schurer et al. 1991), whereas cell membranes are mainly composed of phospholipids. The SC forms a continuous sheath of alternating protein-enriched

A. Ruettinger · R. H. H. Neubert (✉)
Institute of Pharmacy, Martin-Luther-University,
Wolfgang-Langenbeck-Str. 4, 06120 Halle (Saale), Germany
e-mail: Reinhard.Neubert@pharmazie.uni-halle.de

M. A. Kiselev · A. M. Balagurov
Frank Laboratory of Neutron Physics,
Joint Institute for Nuclear Research,
Dubna, Moscow Reg, Russia

Th. Hauss · S. Dante
Hahn-Meitner-Institute, Berlin, Germany

corneocytes that are embedded in an intercellular multilamellar lipid matrix.

According to Wertz and van den Bergh (1998) the SC represents the main barrier for substances leaving the skin, for example water, in addition to also acting as a barrier for substances, which penetrate the skin such as drugs. Therefore, for any investigation of drug penetration through the SC and for the development of new delivery systems, it is essential to know its internal nanostructure and hydration behaviour on a molecular level. It is well known that the SC serves as barrier to transepidermal water loss (TEWL) (Lampe et al. 1983a, b). It was however, not until a series of experiments had been carried out before it was accepted that the lipid part of the SC plays an important role in the function of this barrier. With freeze-fracture electron microscopy a broad, multiple membranous structure was identified (Elias and Friend 1975) and it became evident that this structure fills most of the intercellular part of the SC.

It is not the individual lipid species, which determine the barrier against transcutaneous water loss, but the organisation of the lipids as well as the corneocytes (Friberg et al. 1990). The ability of lipids to form bilayers and multilamellar structures is believed to be responsible for the water retention function and permeability barrier for drugs. To prove this point it is possible to show that a total extraction of lipids with organic solvents results in an increased permeability of the barrier (Sweeney and Downing 1970).

A series of events such as the increased synthesis of fatty acids (Grubauer et al. 1987), sphingolipids (Holleran et al. 1991) and sterols (Feingold et al. 1990; Menon et al. 1985) are initiated after a perturbation of the SC lipids due to application of organic solvents in order to restore the SC barrier function. Mao-Qiang and co-workers found that after barrier disruption and inhibition of the fatty acid synthesis, the recovery of the barrier function is less pronounced demonstrating thereby the necessity of FFA within the SC for a normal barrier function. After application of additional FFA, the barrier recovery improves (Mao-Qiang et al. 1993). The most abundant FFA in human SC are the 22- and 24-carbon entities (Bonte et al. 1997; Norlen et al. 1998; Weerheim and Ponec 2001). Aside from the small amount of cholesterol sulphate, the FFA are the only ionisable lipids in the SC, this may be important for the formation of lamellae.

Many studies have been performed in order to receive more detailed information about the internal nanostructure of the SC and its properties. In previous studies it has been shown that X-ray and neutron scattering are very powerful tools for the investigation of the nanostructure of isolated SC (Bouwstra et al. 1995, 1991, 1994) as well as SC model membranes constructed from extracted SC lipids (Bouwstra et al. 1999, 1996, 2001, 1998, 1997; Friberg and Osborne 1987; Kuempel et al. 1998; McIntosh 2003; McIntosh et al. 1996). In 1988, White and co-workers found a periodicity of 130 Å for the lipid matrix of the SC (White et al. 1988). The brick and mortar model of the SC proposed by Elias (1981) was supported by the results received from small angle neutron scattering experiments (Charalambopoulou et al. 2000).

The calculation of the scattering length density profile received from neutron and X-ray experiments allows for analysis of the internal structure of the SC lipid membrane as well as the water distribution function. It is generally accepted that the hydration level of the SC lipid matrix can influence the penetration of substances through the SC (Fritsch and Stoughton 1963; Idson 1975; Scheuplein 1978; Zimmerer et al. 1986). Therefore, to gain insights into the water distribution through the SC lipid matrix and its manipulation is mandatory.

The utilisation of SC model membranes offers the unique possibility to gain a closer look into the structural assembly of the SC lipids. Using synthetic lipids is advantageous as issues due to the variability of the native lipids can be overcome. Model membranes enable a systematic study of the impact of different lipids on the assembly and structural properties of the membranes. Many efforts have been undertaken to investigate the structure of the model membranes based on nine types of ceramides (Bouwstra et al. 1999, 1996, 1997; Pilgram et al. 1998; Ponec et al. 2000). Nevertheless, the information about the nanostructure was limited to the determination of the repeat distance. The application of a more simplistic, but realistic model membrane based only on one type of ceramide gives an insight into the internal nanostructure of the lipid bilayer (Kiselev et al. 2005).

A model membrane system containing a realistic mixture of different FFA cannot give detailed information about the influence of *each* FFA species and does not provide any indication about the influence of chain length of the FFA to the structure of such SC lipid model membranes. In preceding experiments unique information was obtained with model membranes based on CER[AP] containing palmitic acid (Kiselev et al. 2005). Therefore, the variation of the FFA chain length in this model membrane can give precise information about structural role of *each* FFA used. From this point of view this work is a prolongation of our previous study (Kiselev et al. 2005).

Materials and methods

Materials

The SC lipids used for the model preparation were ceramide [AP] (*N*-(α-Hydroxyoctadecanoyl)-phytosphingosine,

CER [AP]), kindly donated by Cosmoferm (Delft, The Netherlands), stearic acid, docosanoic acid (further referred as behenic acid), tetracosanoic acid, hexacosanoic acid (further referred as cerotic acid), as well as cholesterol and cholesterol sulphate were obtained from Sigma–Aldrich (Taufkirchen, Germany). Quartz slides (Spectrosil 2000) were purchased from Saint-Gobain (Wiesbaden, Germany).

Sample preparation

The SC model membranes were studied in four different compositions; however, only the FFA was changed as shown in Table 1. The ratio of the lipids chosen were similar to the ratio of ceramide, cholesterol and FFA found in the native SC (Wertz 2000) and to the composition used by Wertz and co-workers (1986) as well as Hatfield and Fung (1995). The appropriate amount of each lipid was dissolved in a chloroform:methanol mixtures (2:1) to produce a lipid mixture with a total lipid concentration of 10 mg/ml. The deposition of multilayer lipid films were performed from organic solution according to Seul and Sammon (1990). A volume of 1,200 µl was spread over the surface of a quartz slide with the dimensions of 6.5 cm × 2.5 cm. The organic solvent was removed firstly by evaporation at atmospheric pressure and then under vacuum. The thickness of the lipid film on the quartz slide is 7.5 µm.

Our main purpose in the sample preparation is to create a one-dimensional liquid crystal with approximately 1,600 membrane layers and a mosaicity about 0.1°. Such well oriented samples can give up to 4–5 diffraction orders in the neutron diffraction experiment, which allows the application of the Fourier analysis for the synthesis of the neutron scattering length density across the membrane. For many years this technique has been used for the characterisation of phospholipid membranes (Wiener and White 1991; Worcester 1976).

To decrease the mosaicity of the samples a subsequent heating (at 75°C) and cooling cycle was applied, whereby the sample was kept in horizontal position and at 100% relative humidity. This annealing procedure was necessary in order to obtain a better orientation of the membranes and increase the size of the liquid crystal domains.

Table 1 Composition of the quaternary system for the SC model membrane based on CER[AP]

Mixture	Free fatty acid (FFA)	Component ratio (w/w) (CER[AP]/Ch/FFA/ChS
QuatSA	Stearic acid	55/25/15/5
QuatBA	Behenic acid	57/24/9.5/9.5
QuatTA	Tetracosanoic acid	55/25/15/5
QuatCA	Cerotic acid	55/25/15/5

The SC model membrane was always composed of CER[AP]/Ch/FFA/ChS. Only the FFA component was varied

X-ray diffraction measurements

The X-ray diffraction patterns were collected using the Stoe Stadi MP Powder diffraction system (STOE & Cie GmbH, Darmstadt, Germany) in the Bragg-Brentano high-resolution mode with a linear PSD detector. The samples were measured in vertical position at room temperature and room humidity.

Neutron diffraction measurements

The neutron diffraction measurements were carried out using the membrane diffractometer V1 at the Berlin Neutron Centre of the Hahn-Meitner-Institute, Berlin, Germany with a cold source and a neutron wavelength of $\lambda = 5.23$ Å. A two-dimensional position sensitive ^{3}He detector with a sensitive area of 19 cm × 19 cm and a pixel size of 1.5 mm × 1.5 mm was used ($\Delta x_d = 1.5$ mm). The sample to detector distance L_{sd} amounts to $L_{sd} = 101.8$ cm. The neutron diffraction in the reflection setup was used to collect the data of the one-dimension diffraction experiment. A basic sketch of the scattering geometry is presented in Fig. 1.

According to the standard diffraction notes, 2θ is the angle between the direction of the incident beam (transmitted beam) and the reflected beam, which is same as the angle between the vectors $\vec{k}$ and $\vec{k}'$ (see Fig. 1). We consider an elastic scattering process, $|\vec{k}| = |\vec{k}'|$, thus the

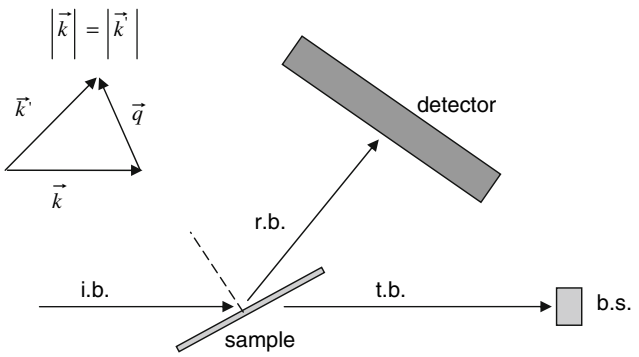

Fig. 1 Sketch of experiment geometry, whereby *i.b.* is incident beam, *r.b.* is reflected beam, *t.b.* is transmitted beam, *b.s.* is beam stop. $\vec{k}$ and $\vec{k}'$ are the wave vectors of the incident and reflected neutrons, $\vec{q}$ is scattering vector

absolute value of the scattering vector q (momentum transfer) can be written as

$$q = \frac{4\pi \cdot \sin(\Theta)}{\lambda} \quad (1)$$

The integrated intensity of the diffraction peak depends on the number of layers N in the lipid film and is proportional to N^2. The width of the diffraction peak Δq depends on the resolution of the instrument Δq_1 and sample mosaicity Δq_2. The mosaicity of the sample is a property of mixed lipids and a result of the sample preparation, whereas the resolution of the instrument depends on the monochromator quality ($\Delta\lambda/\lambda \approx 0.01$), the angle resolution of the detector $\Delta\Theta = \frac{\Delta x_d}{L_{sd}}$, and Bragg's angle θ

$$\frac{\Delta q_1}{q_1} = \sqrt{\left(\frac{\Delta\lambda}{\lambda}\right)^2 + \left(\frac{\Delta\Theta}{\Theta}\right)^2} \quad (2)$$

The linear absorption coefficients for the diffraction order h depend on Bragg's angle θ, linear absorption of lipid film μ and thickness of the film L (Franks and Lieb 1979):

$$A_h(\Theta) = \left[\frac{\sin\Theta}{2\mu L} \cdot \left(1 - \exp\left(-\frac{2\mu L}{\sin\Theta}\right)\right)\right]^{-\frac{1}{2}} \quad (3)$$

It was shown by Kiselev and co-workers that for SC lipid film with a thickness of $L = 7.5$ μm the values of $A_h(\theta)$ are equal to 1.05, 1.02, 1.02, 1.01, 1.01 and 1.01 for the diffraction orders $h = 1, 2, 3, 4, 5$ and 6, respectively (Kiselev et al. 2005). We can therefore neglect the corrections of the absorption for $L = 7.5$ μm. The absorption effect together with the mosaicity of the sample limits the integrated intensity of the diffraction peak, thereby limiting the number of analysable diffraction peaks altogether.

The sample was thermostated in aluminium cans in which the humidity was controlled using an aqueous saturated KBr solution. This procedure is described in detail elsewhere (Hauss et al. 2002). In order to vary the difference in the scattering length density between the lipid membrane and water (neutron contrast), the atmosphere of the sample chamber was adjusted up to four different H_2O/D_2O molar compositions (92/8, 80/20, 50/50 and 0/100). An equilibration time of 12 h was allowed after each change of aqueous solution.

The Fourier synthesis of the scattering length density profile can be calculated on the basis of the measured scattering intensity of the diffraction peaks and the knowledge of the phases of the structure factors (see Eq. 5). It was shown that for symmetrical and hydrated bilayers (Franks and Lieb 1979) the phase problem simplifies to the determination of the structure factor sign of + or −. In contrast to X-ray diffraction, the neutron scattering from lipid bilayers has the principal advantage that the sign of the structure factor can be easily obtained. The sign was determined via measurements of the same sample in water vapour with different contents of D_2O (contrast variation) (Wiener and White 1991). In case of X-rays, the assignment of the sign is a more complex challenge. It could be solved by the application of the sample theorem for the swelling or similar experiment as described by Franks and Lieb (1979).

In our experimental setup the diffraction intensities were recorded either as

(a) $\theta - 2\theta$-scan (high mosaicity samples), or as
(b) rocking scan (ω-scan), whereby the sample was rocked around the expected Bragg position, θ, by $\theta \pm 2°$. This allowed the collection of up to five orders of diffraction as demonstrated in Fig. 2.

Before the collection of the diffraction data of the sample, the rocking curve was checked. A Gaussian-type rocking curve is evidencing a one-dimensional crystal. Two examples are illustrated in Fig. 3, where the left rocking curve (a) belongs to a sample with low mosaicity, which is suitable for a rocking scan. Figure 3b, on the other hand demonstrates a sample with high mosaicity, for which the diffraction intensity could only be recorded as $\theta - 2\theta$-scan.

All measurements were carried out at $T = (20 \pm 0.1)$°C and 57% relative humidity (RH) after 12 h of equilibration in above-mentioned thermostated chamber.

Evaluation of the neutron diffraction data

The measured intensities, recorded either as rocking scans or as $\theta - 2\theta$-scan from the oriented multilamellar lipid

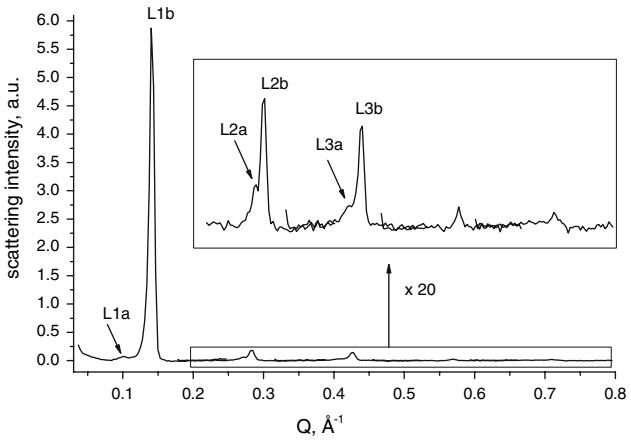

Fig. 2 Diffraction pattern for the quaternary SC model membrane composed of CER [AP]/Ch/BA/ChS (57/24/9.5/9.5). Measured at five different detector angles (6.7, 13.4, 20.1, 26.8, 33.5), at 57% RH, 8% D_2O and 20°C. Up to five orders of diffractions are visible. The orders 2–5 are zoomed by a factor of 20 to the right intensity scale. For phase 1_small (**a**) and phase 2_main (**b**) the first, second and third diffraction orders have been indicated for better understanding, respectively

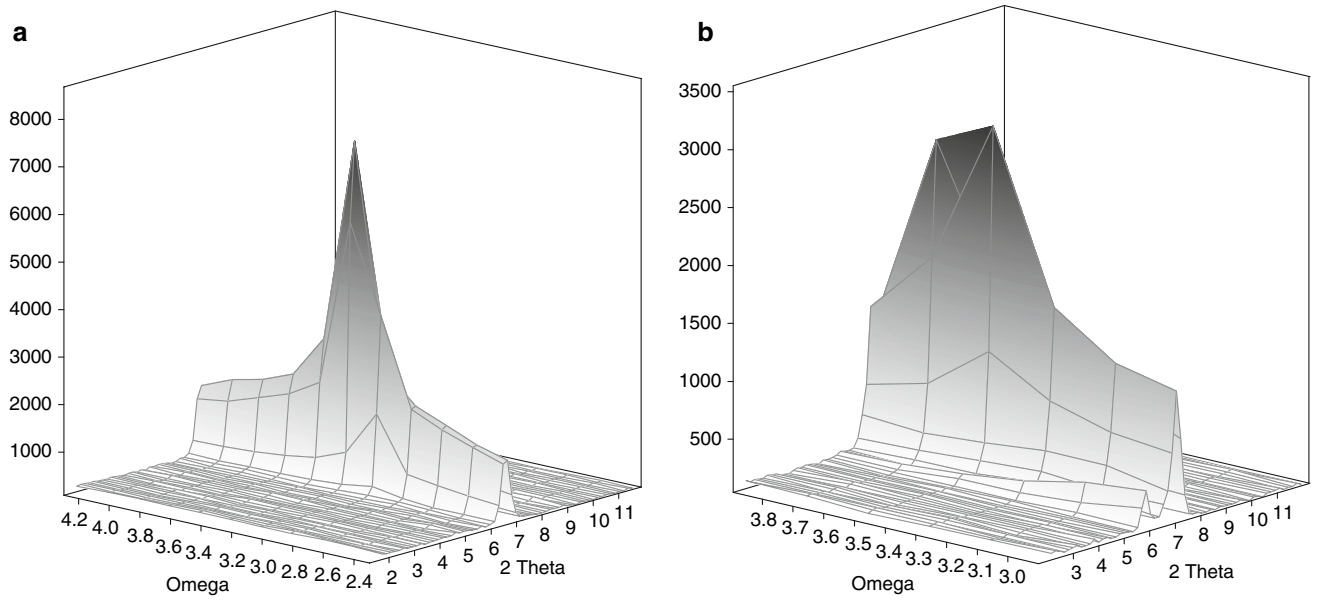

Fig. 3 Rocking curve around a fixed angle 2θ to verify the mosaicity of the sample. **a** Example for a sample with a low mosaicity, which allowed recording of a rocking scan around the expected Bragg position. **b** Illustration of a sample with a high mosaicity for which the diffraction intensities could only be recorded as a θ–2θ-scan

systems revealed up to five diffraction orders, which allowed the application of the Fourier synthesis for the description of the internal membrane structure as shown previously (Kiselev et al. 2005). The absolute value of the structure factor for each diffraction order was determined according to:

$$|F_h| = \sqrt{hI_h} \tag{4}$$

where h is the diffraction order and I_h is the integrated peak intensity (Nagle and Tristram-Nagle 2000). The program PeakFit was used for background subtraction, calculations of the peak intensities and the following fitting procedure.

Bimolecular lipid membranes composed of two equal monolayers facing each other are centrosymmetric bilayers, for which the sign of the structure factor can be determined by isotopic substitution of H_2O by D_2O and assuming the penetration of water into the bilayer (Franks and Lieb 1979; Worcester 1976). The sign of the structure factor was derived from the slope of the correlation of F_h against the D_2O content in water vapour as shown in Fig. 4. The neutron scattering length density profile $\rho(x)$ across the bilayer was calculated by Fourier synthesis according to Nagle and Tristam-Nagle in order to receive nano-structural information (Nagle and Tristram-Nagle 2000):

$$\rho_s(x) = a + b\frac{2}{d}\sum_{h=1}^{h_{\max}} F_h \cos\left(\frac{2\cdot\pi\cdot h\cdot x}{d}\right) \tag{5}$$

The terms a and b in Eq. (5) are free coefficients, which are unknown, F_h is the scaled structure factor of the order h. The last term of Eq. (5) describes the distribution of scattering length density across the bilayer (Fourier profile), whereby d expresses the length of the unit cell. The scattering length density across the bilayer $\rho_s(x)$ is calculated in arbitrary units due to the unknown values of a and b (Nagle and Tristram-Nagle 2000). The Fourier profiles shown further on, had been scaled relatively to each other because of lacking values for a and b. The presented Fourier profiles were all measured at 8, 20, 50 and 100% D_2O in water vapour, respectively, whereby 8% D_2O corresponds to the zero scattering length density of water. At 8% D_2O a typical lipid membrane profile shows two maxima that are related to the phytosphingosine as well as the carboxylate backbone (which therefore represents the headgroups of the lipids) and a minimum at the centre of the bilayer, corresponding to the terminal methyl groups of the lipids.

For normalisation of the scattering length density the values of the methyl (-0.087×10^{11} cm^{-2}) and methylene groups (-0.030×10^{11} cm^{-2}) were used. From previous studies (Kiselev et al. 2005) it is known that the centre of the membrane at $x = 0$ is only formed by CH_3 groups. Therefore, and for simplicity, the centre of the membrane was arranged at $\rho_s(x) = -1$ in arbitrary units. Further, the only CH_2 containing CH_2-region was used for the relative scaling, they were arranged at -0.34, which in our arbitrary scale corresponds to the $\rho_s(x) = -0.030 \times 10^{11}$ cm^{-2}. This normalisation was performed for each Fourier profile, consequently the profiles are presented in arbitrary units but on the same scale.

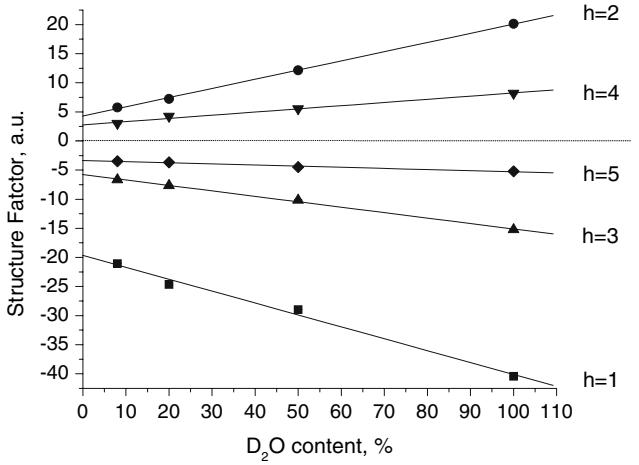

Fig. 4 Example of the dependency of the membrane structure factor F_h of the order h = 1, 2, 3, 4 and 5 on the D_2O content in water vapour for phase 2_main of the quaternary system composed of CER [AP]/Ch/BA/ChS (57/24/9.5/9.5) at 20°C and 57% RH

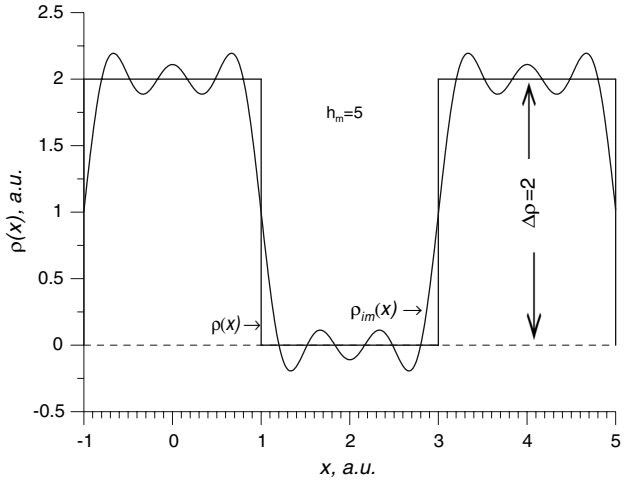

Fig. 5 Truncation errors of the Fourier synthesis based on five diffraction orders as described in Kiselev et al. (2006). The step function $\rho(x)$ is an example of neutron length density profile. The term $\rho_{im}(x)$ is the Fourier synthesis model of the periodic step function $\rho(x)$ based on 5 diffraction peaks

Truncation errors of the Fourier synthesis

The full Fourier transformation from reversed space to direct space requires the knowledge of the structure factors for the diffraction orders h from zero to infinity. In the experiment only a limited number of diffraction peaks can be acquired resulting in a limited set of structure factors. The application of such a limited number of summands in Eq. (5) causes the truncation errors in the application of Fourier transformation to the experimental data. The deviation of the calculated values of the scattering density from the real density distribution shows mainly two effects: the resolution is diminished and at the edges of sharp density change additional oscillations as artefacts are produced. To estimate the influence of the truncation errors Kiselev and co-workers (2006) compared a periodic step function $\rho(x)$, with its Fourier image $\rho_{im}(x)$. In this model calculation assumed relative variables have been used which are comparable to the variables available from the neutron diffraction experiment. Figure 5 represents such a periodical step-function $\rho(x)$ and its Fourier image $\rho_{im}(x)$, which was synthesised on the basis of five structure factors ($h_{\max} = 5$) as

$$\rho_{im}(x) = \frac{F_o}{d} + \frac{2}{d}\sum_{h=1}^{h=5} F_h \cdot \cos\left(\frac{2 \cdot \pi \cdot h \cdot x}{d}\right), \tag{6}$$

with the structure factors F_h given by

$$F_h = \frac{d \cdot \Delta\rho}{\pi \cdot h} \mathrm{Sin}\left(\frac{\pi \cdot h}{2}\right) \text{ and with } F_o = \frac{d \cdot \Delta\rho}{2} \tag{7}$$

whereby $\Delta\rho = 2$ and $d = 6$ are relative values used for the model calculation (see Fig. 5). As can be seen in Eq. (7), the amplitude of the harmonic functions is proportional to the value of $\Delta\rho$. Higher harmonics create the main part of the truncation errors near the sharp boundaries as seen in Fig. 5.

The truncation errors were considered as the difference between the real $\rho(x)$ step-function and experimentally obtained scattering length density $\rho_s(x)$, which was obtained after the Fourier synthesis.

Limited space resolution allows distinguishing two different molecular groups in the experiment *only* if the distance Δx between these groups is equal or larger then:

$$\Delta_{\mathrm{FS}} = \frac{3.8 \cdot d}{2\pi \cdot h_{\max}} \approx 0.6\frac{d}{h_{\max}}, \tag{8}$$

where Δ_{FS} is the space resolution of the Fourier synthesis and d is the membrane repeat distance (Kiselev et al. 2005).

The differences in the value of $\rho(x)$ and $\rho_s(x)$ in Fig. 6 at a given value of x are such truncation errors due to the limited number of diffraction peaks received in the experiment. The truncation error near the sharp boundary is proportional to the value of the boundary density contrast $\Delta\rho$. In neutron diffraction experiments on hydrated lipid membranes, the value of $\Delta\rho$ (value of contrast) can be varied by increasing the D_2O content in the water vapour. Thus, increasing of the contrast could increase the value of truncation errors of the Fourier synthesis at a fixed space resolution.

Results

Behenic acid based SC model membranes

The stratum corneum model membranes based on ceramide [AP] (CER[AP]) and containing behenic acid (22 C-atoms)

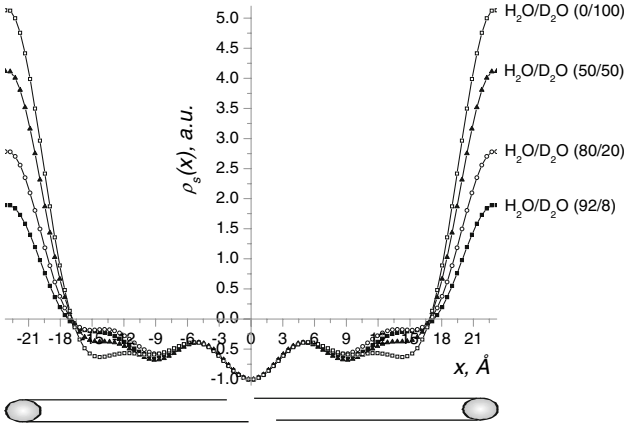

Fig. 6 The neutron scattering length density profiles $\rho_s(x)$ of phase 1_small of the quaternary membrane composed of CER [AP]/Ch/BA/ChS (57/24/9.5/9.5) at different D_2O-contents (8, 20, 50 and 100%), measured at 57% RH and 20°C. At the bottom a pair of CER[AP] molecules is shown, for orientation

as the fatty acid component exhibit a mosaicity inferior to 0.11°, which is similar to membranes based on palmitic acid [mosaicity 0.12°, (Kiselev et al. 2005)] demonstrating the excellent quality of the samples. Due to this excellent sample quality 5 orders of diffraction peaks could be collected. Figure 2 represents the diffraction pattern of the SC model membrane containing behenic acid. The final background subtraction was done within the PeakFit program for the evaluation of the scattering intensity. The presented diffraction pattern in Fig. 2 was created from rocking curves with partial background subtraction.

Membranes containing palmitic acid as the fatty acid component only exhibit one phase at 57% RH and room temperature, a second phase appears at a temperature of 81°C and an increased relative humidity of 97% (Kiselev et al. 2005). In contrast the membranes containing behenic acid, two phases already coexist at 20°C and 57% RH as seen in Fig. 2, where the first diffraction peak exhibits a small shoulder. For clarity, each phase was given a name: the left phase was named phase 1_small (because of smaller scattering intensity), the other is named phase 2_main because it resembles the main intensity. For each phase the calculations were done separately in order to make a comparison of the structure and analyse the difference between both phases. The membrane repeat distance d was determined for each phase from the position of the peaks. For phase 1_small it amounts to $d_1 = (45.5\ \text{Å} \pm 0.3)\ \text{Å}$ and for phase 2_main $d_2 = (44.00\ \text{Å} \pm 0.02)\ \text{Å}$. Note that the average repeat distance $\bar{d} = (44.9 \pm 0.3)\ \text{Å}$ is different from the repeat distance of the main phase, d_2. Consequently, the small phase has a significant influence on the average repeat distance. The repeat distance characterises the membrane spacing without detailed information about the internal structure of the bilayer.

The calculations of the $\rho_s(x)$ function were done separately for the main phase, and the small phase. Figure 6 represents the neutron scattering length density profiles of phase 1_small for 8, 20, 50 and 100% D_2O. The left and right maxima in the profiles are related to the hydrophilic headgroups of the bilayer. The scattering length density in the region of the headgroups increases with increasing D_2O concentration because the D_2O molecules are able to penetrate into the hydrophilic region. The lower values of $\rho_s(x)$ within the profiles resemble the hydrophobic inner part of the membrane, that is, the hydrocarbon chain of the lipids which consist of methylen and methyl groups. The differences in the scattering length density profile for different D_2O concentrations in the middle part are due to truncation errors of the Fourier synthesis. Maximum truncation errors exist at 100% D_2O due to the greatest difference in the scattering density between the hydrated polar headgroups and the hydrophobic region. The origin of this problem is presented in Fig. 5. As shown in Fig. 5, the sharp barrier of the hydrophobic–hydrophilic (HH) boundary transforms to a smooth curve with oscillations. For $h_m =$ constant, the amplitude of these oscillations depends on the value of the barrier (Kiselev et al. 2006). In our case the difference in the scattering length density between the hydrophobic and the hydrophilic regions increases as the D_2O content increases, see Fig. 6. This phenomenon is explained in detail in the section "Truncation errors of the Fourier synthesis". In contrast to the Fourier profile of phase 1_small the neutron scattering length density profile of phase 2_main (Fig. 7) does not show such pronounced truncation errors because the intensity of the first order diffraction peak for the main phase is sufficiently larger relative to the small phase. The consequence is a better signal to noise ratio. Both profiles show no principal differences in the internal alignments of the lipid molecules.

The neutron scattering length density profile across the bilayer gives information about the position of the different groups within the bilayer. The model of the SC membrane structure based on the headgroups, CH_3 group, hydrocarbon chain region, and region of cholesterol location was proposed by Kiselev (Kiselev et al. 2005). It was shown that to gain quantitative information about the internal structure it is possible to fit the Fourier profile with Gaussian functions. Four functions were used for the fitting and characterisation of the four different groups existent within the bilayer. For the position of the methyl group only one Gaussian function is required as this group is centred at $x = 0$ as described earlier. The parameters for the fit resemble the area A and the standard deviation σ. As those bilayers are centrosymmetric it is possible to fit the headgroups and the methylen chains as well as the position

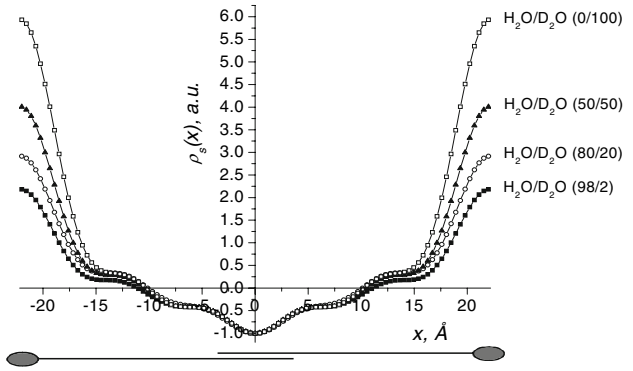

Fig. 7 The neutron scattering length density $\rho_s(x)$ of phase2_main of the model membrane composed of CER [AP]/Ch/BA/ChS (57/24/9.5/9.5) at different D_2O-contents (8, 20, 50 and 100%), measured at 57% humidity and 20°C. In this case, 2 overlapping FA-molecules have been included at the bottom for better demonstration

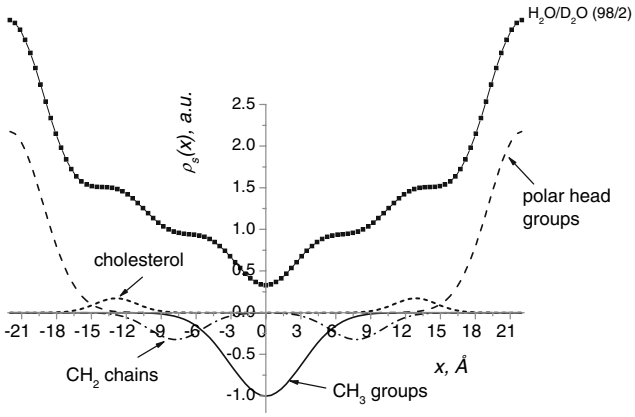

Fig. 8 Model calculations of the neutron scattering length density $\rho_s(x)$ of phase 2_main of system containing behenic acid. The *fitted curves* for each group: polar headgroups (*dash*); CH_2-groups (*dash-dot*), CH_3-group (*solid line*), cholesterol (*short dash*)

of the cholesterol molecules in the bilayer using Eq. (9) for each group.

$$\rho^{\mathrm{sym}}(x)=\frac{A}{\sqrt{2\pi\sigma}}\left\{\exp\left[-\frac{1}{2}\left(\frac{x-x_0}{\sigma}\right)^2\right]+\exp\left[-\frac{1}{2}\left(\frac{x-x_0}{\sigma}\right)^2\right]\right\} \tag{9}$$

In Fig. 8 the neutron scattering profiles in addition to the fitted functions for each group are displayed for phase 2_main of the quaternary membrane based on CER[AP] containing behenic acid. The thickness of the headgroup region equals FWHH/2, where full width at half height (FWHH) is given by (Gordeliy and Kiselev 1995)

$$\mathrm{FWHH} = 2 * \sigma\sqrt{2 * \ln 2} \tag{10}$$

The same fitting procedure of the neutron scattering length density profile for phase 1_small was performed (data not shown). For both phases the parameters taken from the fit differ only marginally due to experimental errors. As a consequence, although phase 1_small and phase 2_main show different repeat distances, the structural alignment of the lipids within both phases is similar. Therefore, the difference in the thickness of the membrane between phase 1_small and phase 2_main is due to a different composition of the lipids inside both phases.

As already described by Kiselev and co-workers (2005), the SC lipid model membrane based on ceramide [AP] and with palmitic acid as fatty acid component does not show a region of intermembrane space in contrast to phospholipids (Kiselev et al. 2005). As described for the case of phase 1_small, also for phase 2_main the membrane repeat distance d is equal to the distance between the two maxima of the polar headgroups d_{PH}. The headgroups of the different leaflets are arranged close to each other. The thickness of the intermembrane space amounts to approximately zero at 57% RH. The region, which is hydrated by the water molecules is very small, therefore the intermembrane space of such model membranes is not suitable for lateral water diffusion in addition to the lateral diffusion of drugs. This can be a reason for the low penetration rates of drugs through the stratum corneum. On the other hand, our results show, that lamellar diffusion of water and water soluble drugs is preferred relative to lateral diffusion because hydration of the internal part of the bilayer appears to be very similar to that of phospholipids (Kiselev et al. 2005).

The dependence of the Fourier profile on the D_2O content in water vapour enables the calculation of the water distribution ρ_w across the bilayer as the difference between the neutron scattering density at high D_2O concentration (50 and 100%) and 8% D_2O in water vapour according to the Eqs. (11a) and (11b). For both phases calculation were done. The result for phase 2_main is presented in Fig. 9.

$$\rho_{w1} = \rho_{100\%\mathrm{D_2O}} - \rho_{8\%\mathrm{D_2O}} \tag{11a}$$

$$\rho_{w2} = \rho_{50\%\mathrm{D_2O}} - \rho_{8\%\mathrm{D_2O}} \tag{11b}$$

Again, phase 1_small gives the same water distribution function as phase 2_main (data not shown) which further underlines the conclusion, that both phase do not show a difference in the structural alignment of the lipids rather a different composition of the lipid.

The membrane can be divided into two parts, namely the hydrophilic and hydrophobic region. Thus, the boundary between both regions can be described as HH boundary and is located at the position x where the water distribution function ρ_w is near to zero. The HH boundary determines the thickness of the hydrophilic part of the bilayer. The position of the HH boundary for each phase is summarised in Table 2. In order to prove the accuracy of this method the difference between 100 and 8% D_2O was compared with the difference between 50 and 8% D_2O. The

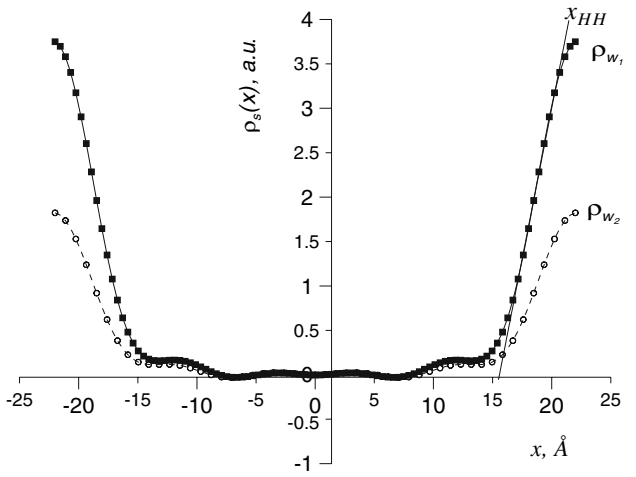

Fig. 9 Water distribution function $\rho_w(x)$ of phase 2_main across the CER [AP]/Ch/BA/ChS membrane. *HH* boundary is determined via linear fit as demonstrated here

comparison of both calculated values gave an accuracy of 0.2 Å for the method used.

Stearic acid based membrane

The model membrane containing stearic acid as FFA component was also characterised by neutron diffraction in order to gain more information about the influence of the chain length of the FFA in the SC model membrane. Comparable to the sample containing behenic acid the low mosaicity of this model membrane (0.10°) allowed the collection of 5 orders of diffraction peaks at a temperature of 20°C, 57% RH and 8, 20 and 50% D_2O concentration in water vapour, respectively. As described for the membrane containing behenic acid, this membrane also shows a coexistence of two phases at 20°C. In contrast to the system based on behenic acid, the phase separation cannot be observed in the first diffraction peak because the intensity of the first phase is substantially larger than that of the second phase. Again, for clarity each phase was named according to the extent of its scattering intensity: the first phase was named phase 1_main, the other was named phase 2_small as it has a very small scattering intensity relative to the main phase. As described previously, the calculations were done independently for each phase in order to make a comparison of the structure. The membrane repeat distance d was determined for each phase from the position of the peak. For phase 1_main it amounts to $d_1 = 46.3$ Å $\pm$ 0.02 Å and for phase 2_small $d_2 = 45.3$ Å $\pm$ 0.2 Å. The presentation of the results will be limited to the main phase.

The neutron scattering length density profile $\rho_s(x)$ across the bilayer was calculated for each phase separately as Fourier synthesis. Similar to the membranes containing palmitic acid (Kiselev et al. 2005) or behenic acid, the membrane including stearic acid does not show a region of intermembrane space. For both phases the membrane repeat distance d is equal to the distance between the two maxima of the headgroups d_{PH}, therefore the thickness of the intermembrane space amounts to approximately zero at 57% RH, which corresponds to the organisation as described for the systems with palmitic (Kiselev et al. 2005) and behenic acid.

The calculation of the water distribution function across the bilayer produced similar results as described for the model membrane containing behenic acid. No significant difference between phase 1_main and phase 2_small could be detected, which again proves the assumption that there is no difference in the structural assembly of both phases. The quantitative information about the internal structure was received by fitting the Fourier profile as described above, the major results for the main phase are summarised in Table 3. The results show that the membrane structure is not altered due to variation of chain length from C22:0 (BA) to C18:0 (SA). To further prove this, longer fatty acids where used.

Tetracosanoic acid based membrane

The fatty acids found in the epidermal SC are almost entirely saturated and are longer than 18 carbons in length. The most abundant FFA in human SC are the 22- and 24-carbon entities (Bonte et al. 1997; Elias et al. 1977; Norlen et al. 1998; Weerheim and Ponec 2001). For this reason the quaternary system was investigated with tetracosanoic acid as the fatty acid component. This sample mosaicity was not low enough to measure a

Table 2 Structural parameters for each phase of the membrane containing behenic acid at 20°C, 8% D_2O and 57% RH

Membrane based on behenic acid	$d = d_m$ (Å)	x_{PH} (Å)	x_{HH} (Å)	Thickness of hydrophobic layer (Å)	Thickness of hydrophilic layer (Å)
phase 1_small	45.5 ± 0.3	22.74	17.0 ± 0.3	34.0 ± 0.6	5.7 ± 0.3
phase 2_main	44.0 ± 0.02	22.00	15.7 ± 0.3	31.4 ± 0.6	6.3 ± 0.3

d Repeat distance, d_m membrane thickness, x_{HH} hydrophilic–hydrophobic boundary, x_{PH} position of polar headgroups

Table 3 Structural parameters for each fatty acid containing membrane at 20°C, 8% D_2O and 57% RH

Membrane based on	$d = d_m$ (Å)	x_{PH} (Å)	x_{HH} (Å)	Thickness of hydrophobic layer (Å)	Thickness of hydrophilic layer (Å)
Stearic acid	46.3 ± 0.02	23.14	15.4 ± 0.2	30.9 ± 0.4	7.7 ± 0.2
Behenic acid	44.0 ± 0.02	22.00	15.7 ± 0.3	31.4 ± 0.6	6.3 ± 0.3
Tetracosanoic acid	43.4 ± 0.1	21.43	15.4 ± 0.3	30.8 ± 0.6	6.3 ± 0.3
Cerotic acid	43.7 ± 0.1	21.85	16.3 ± 0.2	32.1 ± 0.4	5.4 ± 0.2

d Repeat distance, d_m membrane thickness, x_{HH} hydrophilic–hydrophobic boundary, x_{PH} position of polar headgroups

rocking curve; however, it was possible to collect five orders of diffraction as a Theta-two-Theta scan.

In contrast to the already described membranes containing behenic or stearic acid, in this model membrane an additional phase with a longer periodicity appeared. This leads to the assumption that the tendency for phase separation increases with increasing chain length. The phases were named in order of the position of their Q value and the extent of their scattering intensity: phase 1_left (smallest Q-value, longest periodicity), phase 2_small (small scattering intensity) and phase 3_main because it resembles the main scattering intensity. Phase 1_left can be clearly separated from the other two phases, for that reason it can be assumed that it is a completely different phase with a different lipid composition. Phase 2_small and phase 3_main on the other hand show an overlapping in the first and second diffraction order, therefore it can be postulated that the structure of these two phases do not differ markedly, as it was described for the cases of the model membranes containing either stearic or behenic acid. To further gain structural information about this system and to prove the hypothesis, that phase 2_small and phase 3_main are structurally similar all phases were regarded as independent phases.

From the position of the diffraction peak the membrane repeat distance d was determined for each phase. It amounts to $d_1 = 51.1$ Å ± 0.8 Å for phase 1_left, for phase 2_small to $d_2 = 44.7$ Å ± 0.3 Å and for phase 3_main to $d_3 = 43.3$Å ± 0.1 Å. Similar to the membranes containing behenic or stearic acid the influence of phase 2_small on the membrane nanostructure is negligibly small. Consequently, only the results obtained for phase 1_left and for phase 3_main will be presented further on. As described above, a neutron scattering length density profile $\rho_s(x)$ across the bilayer was calculated for each phase. Again, the neutron scattering length density profile of the phases 2_small and 3_main do not show any significant differences, meaning that the structural alignment of the lipids of both phases is similar and only the composition of the lipids varies which leads to a slight difference in the repeat distance of both phases. The structural parameters of phase 2_main received from the evaluation of the HH boundary (x_{HH}) of the neutron scattering density profile are presented in Table 3. The calculation of the Fourier profile $\rho_s(x)$ revealed no intermembrane region, the thickness of the intermembrane region amount to approximately zero, as described for the model membranes containing either stearic or behenic acid.

In contrast, the comparison of the neutron scattering length density profiles of phase 1_left with phase 3_main shows marked differences, which confirms the assumption that phase 1_left has a different structural arrangement in comparison to phase 2_small and 3_main. As the repeat distance d_1 of phase 1_left is similar to the repeat distance found for membranes created from pure tetracosanoic acid, it was assumed that phase 1_left is mainly composed of tetracosanoic acid. To prove this point the electron density profile received from pure fatty acid membranes via X-ray diffraction (diffraction data not shown) was compared with the neutron scattering length density profile of phase 1_left which is displayed in Fig. 10. Note, that the structural differences are only minor between the profile taken from pure tetracosanoic acid membranes and that from phase 1_left, which is an evidence that phase 1_left is a tetracosanoic-rich phase. Therefore, it can be stated that the appearance of this phase in a SC model membrane based on CER[AP] and containing tetracosanoic acid is due to the decreased solubility of this long-chain fatty acid inside this SC model membrane.

Cerotic acid based membranes

The longest free fatty acid used in our study was cerotic acid (CA) with 26 C-atoms. The low mosaicity of the sample allowed for the collection of five orders of diffraction peaks, which were recorded as rocking curve.

As described for the membrane containing tetracosanoic acid (TA) this fatty acid also displays an additional, clearly separated phase with a longer periodicity. The tendency for phase separation to increase with the elongation of the FFA chain length is further supported by these findings. Similar to TA, the different phases were named as followed: phase 1_left (smallest Q-value, longest periodicity),

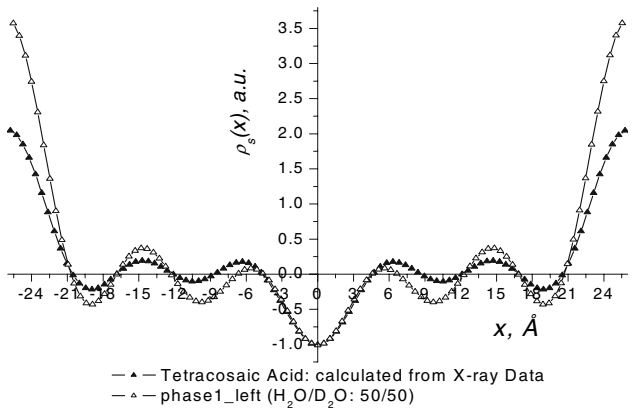

Fig. 10 Comparison of the neutron scattering length density $\rho_s(x)$ of phase1_left of the model membrane containing TA with the electron density profile of a membrane composed of pure tetracosanoic acid

phase 2_small (small scattering intensity) and phase 3_main which represents the main scattering intensity. Again, similar to the membrane with TA, phase 1_left is related to the diffraction from the CA-rich phase.

Once more, the other two phases show an overlapping of the first and second diffraction orders, therefore, it can again be concluded that the composition of those two phases is similar to each other. The membrane repeat distance d was determined for each phase from the position of0the peaks; phase 1_left $d_1 = 56.2$ Å $\pm$ 0.3 Å, phase 2_small $d_2 = 45.5$ Å $\pm$ 0.6 Å and the value for phase 3_main amounts to $d_3 = 43.70$ Å $\pm$ 0.07 Å. Taken this into account, together with the comparison of the calculated neutron scattering length density profiles of phases 2_small and 3_main (data not shown), it can once more be stated that the influence of the second smaller phase is negligibly small to the structure of this model matrix. Consequently, only the results obtained for the calculation of phase 3_main are presented in Table 3. The calculated Fourier profiles revealed as for all the other fatty acids used in this study that this membrane does not show an intermembrane region. The structural results of the SC model membrane containing cerotic acid do not show remarkable differences when compared to the membranes containing one of the other fatty acids used in this study.

Conclusions

The results of the neutron diffraction experiment revealed that the internal nanostructure of the SC model membrane based on ceramide [AP] is not proportionally altered by the increase of the chain length of the free fatty acid (FFA) from stearic (C18:0) to cerotic (C26:0) acid.

The obtained nanostructure for each FFA-containing model membrane investigated in this study is similar to that of the membrane containing palmitic acid (C16:0) (Kiselev et al. 2005). It was observed that an *increase* in the FFA chain length *decreased* the membrane repeat distance, which is demonstrated in Fig. 11. We can explain this unexpected dependency by a partial interdigitation of the chains of the free fatty acids. This interdigitation behaviour may result from the tendency of the fatty acids to "fit" into the membrane size created by ceramide [AP]. The results presented, show that ceramide [AP] creates a super-stable structure, which is not influenced by the alteration of the FFA chain length. The interdigitation of the FFA follows this stability of the membrane. On the other hand this interdigitation creates some free space as shown in Fig. 12. To fill this free space the FFA "pull" the membrane

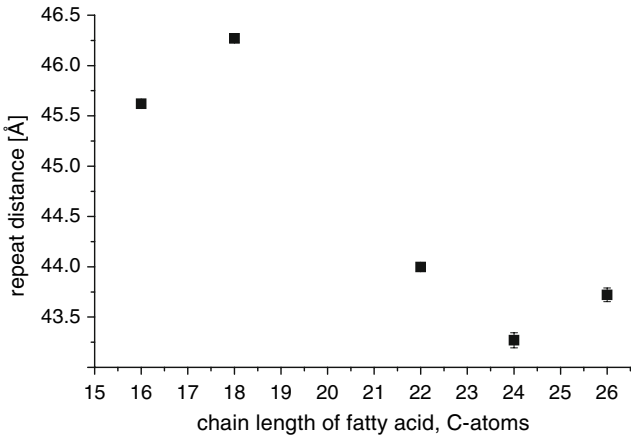

Fig. 11 Membrane repeat distance dependency on the fatty acid chain length. Plotted is the main phase of the different fatty acid containing membranes

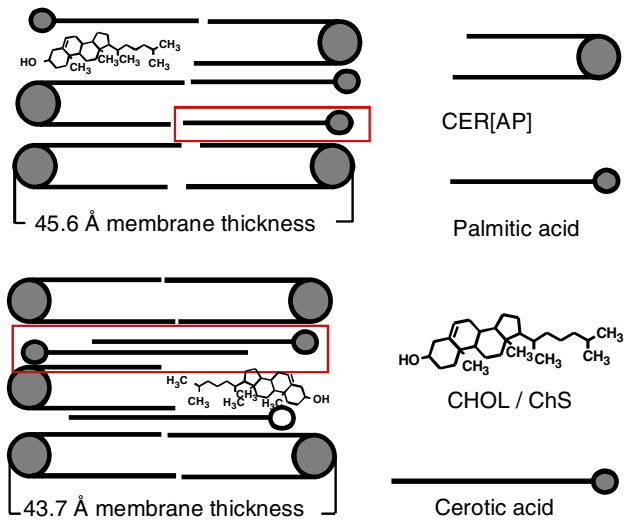

Fig. 12 Schematic presentation of the structural assembly of the SC model matrix. To demonstrate the influence of the longer chained fatty acids a model for the membrane based on palmitic acid is compared with the matrix based on cerotic acid

Table 4 Comparison of the repeat distance *d* of a pure fatty acid membrane with the repeat distance *d* of phase 1_left of the membrane containing either tetracosanoic or cerotic acid

Fatty acid	*d* of pure fatty acid (X-ray) (Å)	*d* of Phase 1_left (Neutron diffraction) (Å)
Tetracosanoic acid	52.6 ± 0.2	51.1 ± 0.8
Cerotic acid	56.5 ± 0.2	56.2 ± 0.3

together. This need to minimize the free volume inside of the membrane can explain the reduction of the membrane thickness when the chain length of the FFA increases.

The term "interdigitation" has been used to describe a phenomenon for phospholipids, whereby pure phospholipids with unequal fatty acid chain length can protrude the methyl group of the leaflet with longer fatty acids amongst the acyl chains of the opposing leaflet (Huang and Mason 1986; Keough and Davis 1979). The use of especially long-chain FFA this SC model membrane is comparable to phospholipids with unequal fatty acid chain length, therefore this phenomenon can be conveyed to the SC model membranes discussed here.

Another finding obtained from our study is that the longer chained FFA, such as tetracosanoic (C24:0) and cerotic acid (C26:0) form a new "fatty-acid-rich phase". This finding can be explained by the decreased solubility of the long chained fatty acids within the SC model membrane based on ceramide [AP]. It was further confirmed by the investigation of pure fatty acid membranes using X-ray diffraction. The phase with the longest periodicity (labelled as phase 1_left) has a similar periodicity to that of the pure fatty acid membranes (Table 4). Furthermore, the structural comparison of the pure fatty acid membrane with either phase 1_left also revealed an alikeness of both membranes (see Fig. 10).

To conclude our research it can be summarised, that the very polar short-chain phytosphingosine-type ceramide [AP] dictates the main phase of this SC lipid model membrane. The interactions created by the ceramide [AP] molecules are the main forces, which determine the stability of this SC model membrane. Therefore, the ceramide obligates the long-chain FFA to either arrange inside this phase or separate as a FFA-rich phase. Further, the appearance of a "fatty-acid-rich phase" indicates that the longer-chained FFA tend towards a formation of a separated phase.

Acknowledgments We would like to thank the members of the group of Prof. Merzweiler for providing the Stoe Stadi MP Powder diffraction system. The work was supported by the Federal State of Saxony-Anhalt, project "Neutron scattering in Biological Systems" (3482A/1102M). Financial assistance from the Hahn-Meitner-Institute (Berlin, Germany) is also gratefully acknowledged. The authors would like to thank Cosmoferm (Delft, The Netherlands) for the donation of CER [AP].

References

Bonte F, Saunois A, Pinguet P, Meybeck A (1997) Existence of a lipid gradient in the upper stratum corneum and its possible biological significance. Arch Dermatol Res 289:78–82

Bouwstra JA, Gooris GS, van der Spek JA, Bras W (1991) Structural investigations of human stratum corneum by small-angle X-ray scattering. J Invest Dermatol 97:1005–1012

Bouwstra JA, Gooris GS, van der Spek JA, Lavrijsen S, Bras W (1994) The lipid and protein structure of mouse stratum corneum: a wide and small angle diffraction study. Biochim Biophys Acta 1212:183–192

Bouwstra JA, Gooris GS, Bras W, Downing DT (1995) Lipid organization in pig stratum corneum. J Lipid Res 36:685–695

Bouwstra JA, Gooris GS, Cheng K, Weerheim A, Bras W, Ponec M (1996) Phase behavior of isolated skin lipids. J Lipid Res 37:999–1011

Bouwstra JA, Thewalt J, Gooris GS, Kitson N (1997) A model membrane approach to the epidermal permeability barrier: an X-ray diffraction study. Biochemistry 36:7717–7725

Bouwstra JA, Gooris GS, Dubbelaar FE, Weerheim AM, Ijzerman AP, Ponec M (1998) Role of ceramide 1 in the molecular organization of the stratum corneum lipids. J Lipid Res 39:186–196

Bouwstra JA, Dubbelaar FE, Gooris GS, Weerheim AM, Ponec M (1999) The role of ceramide composition in the lipid organisation of the skin barrier. Biochim Biophys Acta 1419:127–136

Bouwstra JA, Gooris GS, Dubbelaar FE, Ponec M (2001) Phase behavior of lipid mixtures based on human ceramides: coexistence of crystalline and liquid phases. J Lipid Res 42:1759–1770

Charalambopoulou GC, Karamertzanis P, Kikkinides ES, Stubos AK, Kanellopoulos NK, Papaioannou AT (2000) A study on structural and diffusion properties of porcine stratum corneum based on very small angle neutron scattering data. Pharm Res 17:1085–1091

Elias PM (1981) Lipids and the epidermal permeability barrier. Arch Dermatol Res 270:95–117

Elias PM, Friend DS (1975) The permeability barrier in mammalian epidermis. J Cell Biol 65:180–191

Elias PM, Goerke J, Friend DS (1977) Mammalian epidermal barrier layer lipids: composition and influence on structure. J Invest Dermatol 69:535–546

Feingold KR, Man MQ, Menon GK, Cho SS, Brown BE, Elias PM (1990) Cholesterol synthesis is required for cutaneous barrier function in mice. J Clin Invest 86:1738–1745

Franks NP, Lieb WR (1979) The structure of lipid bilayers and the effects of general anaesthetics. An X-ray and neutron diffraction study. J Mol Biol 133:469–500

Friberg SE, Osborne DW (1987) Interaction of a model epidermal lipid with a vegetable oil adduct. J Dispers Sci Technol 8:249–258

Friberg SE, Kayali I, Beckerman W, Rhein LD, Simion A (1990) Water permeation of reaggregated stratum corneum with model lipids. J Invest Dermatol 94:377–380

Fritsch WC, Stoughton RB (1963) The effect of temperature and humidity on the penetration of C14 acetylsalicylic acid in excised human skin. J Invest Dermatol 41:307–311

Gordeliy VI, Kiselev MA (1995) Definition of lipid membrane structural parameters from neutronographic experiments with the help of the strip function model. Biophys J 69:1424–1428

Grubauer G, Feingold KR, Elias PM (1987) Relationship of epidermal lipogenesis to cutaneous barrier function. J Lipid Res 28:746–752

Hatfield RM, Fung LW (1995) Molecular properties of a stratum corneum model lipid system: large unilamellar vesicles. Biophys J 68:196–207

Hauss T, Dante S, Dencher NA, Haines TH (2002) Squalane is in the midplane of the lipid bilayer: implications for its function as a proton permeability barrier. Biochim Biophys Acta 1556:149–154

Holleran WM, Man MQ, Gao WN, Menon GK, Elias PM, Feingold KR (1991) Sphingolipids are required for mammalian epidermal barrier function. Inhibition of sphingolipid synthesis delays barrier recovery after acute perturbation. J Clin Invest 88:1338–1345

Huang C, Mason JT (1986) Structure and properties of mixed-chain phospholipid assemblies. Biochim Biophys Acta 864:423–470

Idson B (1975) Percutaneous absorption. J Pharm Sci 64:901–924

Keough KM, Davis PJ (1979) Gel to liquid-crystalline phase transitions in water dispersions of saturated mixed-acid phosphatidylcholines. Biochemistry 18:1453–1459

Kiselev MA, Ryabova NY, Balagurov AM, Dante S, Hauss T, Zbytovska J, Wartewig S, Neubert RH (2005) New insights into the structure and hydration of a stratum corneum lipid model membrane by neutron diffraction. Eur Biophys J 34:1030–1040

Kiselev MA, Ryabova NY, Balagurov AM, Otto D, Dante S, Hauss T, Wartewig S, Neubert RHH (2006) Ceramide 6 influence on the structure and hydration of multilamellar dipalmitoylphosphatidylcholine membrane. Poverchnost X-ray Synchrotron Neutron Invest 6:30–37

Kuempel D, Swartzendruber DC, Squier CA, Wertz PW (1998) In vitro reconstitution of stratum corneum lipid lamellae. Biochim Biophys Acta 1372:135–140

Lampe MA, Burlingame AL, Whitney J, Williams ML, Brown BE, Roitman E, Elias PM (1983a) Human stratum corneum lipids: characterization and regional variations. J Lipid Res 24:120–130

Lampe MA, Williams ML, Elias PM (1983b) Human epidermal lipids: characterization and modulations during differentiation. J Lipid Res 24:131–140

Mao-Qiang M, Elias PM, Feingold KR (1993) Fatty acids are required for epidermal permeability barrier function. J Clin Invest 92:791–798

McIntosh TJ (2003) Organization of skin stratum corneum extracellular lamellae: diffraction evidence for asymmetric distribution of cholesterol. Biophys J 85:1675–1681

McIntosh TJ, Stewart ME, Downing DT (1996) X-ray diffraction analysis of isolated skin lipids: reconstitution of intercellular lipid domains. Biochemistry 35:3649–3653

Menon GK, Feingold KR, Moser AH, Brown BE, Elias PM (1985) De novo sterologenesis in the skin. II. Regulation by cutaneous barrier requirements. J Lipid Res 26:418–427

Nagle JF, Tristram-Nagle S (2000) Structure of lipid bilayers. Biochim Biophys Acta 1469:159–195

Norlen L, Nicander I, Lundsjo A, Cronholm T, Forslind B (1998) A new HPLC-based method for the quantitative analysis of inner stratum corneum lipids with special reference to the free fatty acid fraction. Arch Dermatol Res 290:516

Pilgram GS, Engelsma-van Pelt AM, Oostergetel GT, Koerten HK, Bouwstra JA (1998) Study on the lipid organization of stratum corneum lipid models by (cryo-) electron diffraction. J Lipid Res 39:1669–1676

Ponec M, Boelsma E, Weerheim A, Mulder A, Bouwstra J, Mommaas M (2000) Lipid and ultrastructural characterization of reconstructed skin models. Int J Pharm 203:211–25

Scheuplein RJ (1978) Permeability of the skin: a review of major concepts. Curr Probl Dermatol 7:172–186

Schurer NY, Plewig G, Elias PM (1991) Stratum–corneum lipid function. Dermatologica 183:77–94

Seul M, Sammon MJ (1990) Competing interactions and domain-shape instabilities in a monomolecular film at an air–water interface. Phys Rev Lett 64:1903–1906

Sweeney TM, Downing DT (1970) The role of lipids in the epidermal barrier to water diffusion. J Invest Dermatol 55:135–140

Weerheim A, Ponec M (2001) Determination of stratum corneum lipid profile by tape stripping in combination with high-performance thin-layer chromatography. Arch Dermatol Res 293:199

Wertz PW (2000) Lipids and barrier function of the skin. Acta Derm Venereol Suppl (Stockh) 208:7–11

Wertz PW, Abraham W, Landmann L, Downing DT (1986) Preparation of liposomes from stratum corneum lipids. J Invest Dermatol 87:582–584

Wertz PW, van den Bergh B (1998) The physical, chemical and functional properties of lipids in the skin and other biological barriers. Chem Phys Lipids 91:85–96

White SH, Mirejovsky D, King GI (1988) Structure of lamellar lipid domains and corneocyte envelopes of murine stratum corneum. An X-ray diffraction study Biochemistry 27:3725–3732

Wiener MC, White SH (1991) Fluid bilayer structure determination by the combined use of X-ray and neutron-diffraction.1. Fluid bilayer models and the limits of resolution. Biophys J 59:162–173

Worcester DL (1976) Neutron diffraction studies of biological membranes and membrane components. Brookhaven Symp Biol, pp III37–III57

Zimmerer RE, Lawson KD, Calvert CJ (1986) The effects of wearing diapers on skin. Pediatr Dermatol 3:95–101